Power Beacon-Assisted Millimeter Wave Ad Hoc Networks

Xiaohui Zhou, *Student Member, IEEE*, Jing Guo, *Member, IEEE*, Salman Durrani, *Senior Member, IEEE*, and Marco Di Renzo, *Senior Member, IEEE*

***Abstract*— Deployment of low-cost power beacons (PBs) is a promising solution for dedicated wireless power transfer (WPT) in future wireless networks. In this paper, we present a tractable model for PB-assisted millimeter wave (mmWave) wireless ad hoc networks, where each transmitter (TX) harvests energy from all PBs and then uses the harvested energy to transmit information to its desired receiver. Our model accounts for realistic aspects of WPT and mmWave transmissions, such as power circuit activation threshold, allowed maximum harvested power, maximum transmit power, beamforming, and blockage. Using stochastic geometry, we obtain the Laplace transform of the aggregate received power at the TX to calculate the power coverage probability. We approximate and discretize the transmit power of each TX into a finite number of discrete power levels in log scale to compute the channel and total coverage probability. We compare our analytical predictions to simulations and observe good accuracy. The proposed model allows insights into effect of system parameters, such as transmit power of PBs, PB density, main lobe beamwidth, and power circuit activation threshold on the overall coverage probability. The results confirm that it is feasible and safe to power TXs in an mmWave ad hoc network using PBs.**

***Index Terms*— Wireless communications, wireless power transfer, millimeter wave transmission, power beacon, stochastic geometry.**

I. Introduction

WIRELESS power transfer (WPT) can prolong the lifetime of low-power devices in the network and is currently in the spotlight as a key enabling technology in future wireless communication networks [1]–[3]. Compared to energy harvesting from ambient energy sources, e.g., solar, wind or ambient radio frequency (RF) sources, which may change rapidly with time, location and weather conditions, WPT has a significant advantage of being always available and controllable [1]. There are currently two main approaches to WPT: (i) simultaneous information and power transfer (SWIPT) and (ii) power beacon (PB) based approach. While SWIPT, which proposes to extract the information and power from the same signal, has been the subject of intense research in the academic community [1], [4], [5], industry has preferred to adopt the PB approach. In this approach, low cost PBs, which do not require backhaul links, are deployed to provide dedicated power transfer in wireless networks. For example, the Cota Tile is a PB designed to wirelessly charge devices like smartphones in a home environment and was showcased at the 2017 Consumer Electronics Show (CES) [6].

There are two key challenges in the application of PBs to wider networks. The first challenge is the lack of tractable models for analysis and design of such networks. Although simulations can be used in this regard, exhaustive simulation of every possible scenario of interest will be extremely time-consuming and onerous. Hence, it is important to explore tractable models for PB-assisted communications in wireless networks. The second challenge is the use of practical models for WPT, which capture realistic aspects of WPT. For instance, WPT receivers (RXs) can only harvest power if the incident received power is greater than the power circuit activation threshold (typically around -20 dBm [1]). Similarly, WPT transmitters (TXs) have to adhere to maximum transmit power constraints due to safety considerations. Hence, it is important to adopt a realistic and practical model for WPT.

A. Related Work

1) Microwave (Below 6 GHz) Systems: Recently, the investigation of PBs has drawn attention in the literature from different aspects. *For point-to-point or point-to-multipoint communication systems*, the resource allocation for PB-assisted system was considered in [7] and [8], where the authors mainly aimed at finding the optimum time ratio for power transfer (PT) and information transmission (IT). In [9], the authors studied the PB-assisted network in the context of physical layer security, where an energy constrained source is powered by a dedicated PB. For *large scale networks*, some papers have characterized the performance of PB-assisted communications using stochastic geometry, which is a powerful mathematical tool to provide tractable analysis by incorporating the randomness of users. Specifically, the feasibility of PB deployment in a cellular network, under the outage constraint at the base station, was investigated

Manuscript received March 20, 2017; revised September 4, 2017; accepted October 16, 2017. Date of publication October 24, 2017; date of current version February 14, 2018. This work was supported in part by the Australian Research Council under Grant DP170100939 and Grant DP140101133. The associate editor coordinating the review of this paper and approving it for publication was I. Krikidis. *(Corresponding author: Xiaohui Zhou.)*

X. Zhou, J. Guo, and S. Durrani are with the Research School of Engineering, College of Engineering and Computer Science, The Australian National University, Canberra, ACT 2601, Australia (e-mail: xiaohui.zhou@anu.edu.au; jing.guo@anu.edu.au; salman.durrani@anu.edu.au).

M. Di Renzo is with the Laboratoire des Signaux et Systèmes, Centre National de la Recherche Scientifique, CentraleSupélec, University of Paris-Sud, Université Paris-Saclay, 91192 Gif-sur-Yvette, France (e-mail: marco.direnzo@lss.supelec.fr).

Color versions of one or more of the figures in this paper are available online at http://ieeexplore.ieee.org.

Digital Object Identifier 10.1109/TCOMM.2017.2766152

in [10], where cellular users are charged by PBs for uplink transmission. By considering that the secondary TX is charged by the primary user in a cognitive network, the authors derived the spatial throughput for the secondary network in [11]. Adaptively directional PBs were proposed for sensor network in [12] and the authors found the optimal charging radius for different sensing tasks. In [13], three WPT schemes were proposed to select the PB for charging in a device-to-device-aided cognitive cellular network. The authors in [14] formulated the total outage probability in a PB-assisted ad hoc network by including the energy harvesting sensitivity into the analysis. Note that all the aforementioned works considered the conventional microwave frequency band, i.e., below 6 GHz.

2) MmWave Systems: Millimeter wave (mmWave) communication, which aims to use the spectrum band typically around 30 GHz, is emerging as a key technology for the fifth generation systems [15]. Considerable advancements have already been made in the understanding, modelling and analysis of mmWave communication using stochastic geometry [16]–[19]. From the prior work, we can summarize two distinctive features of mmWave communication: (i) owing to the smaller wavelength, mmWave allows a large number of antenna arrays with directional beamforming to be equipped at the TX and RX; (ii) since the mmWave propagation is susceptible to blockage, it causes the large difference for path-loss and fading characteristics between line of sight (LOS) and non light of sight (NLOS) environment.

MmWave communication can be beneficial for WPT since both technologies inherently operate over short distances and the narrow beams in mmWave communication can focus the transmit power. Very recently, some papers have used stochastic geometry to analyse mmWave SWIPT networks [20], [21]. The statistics of the aggregate received power from PBs in a mmWave ad hoc network were studied in our preliminary work in [22]. To the best of our knowledge, the study of a PB-assisted mmWave network using stochastic geometry, taking into account realistic and practical WPT and mmWave characteristics such as building blockages, beamforming, power circuit activation threshold, maximum harvested power and maximum transmit power, is not available in the literature.

B. Our Approach and Contributions

In this paper, we consider a PB-assisted wireless ad hoc network under mmWave transmission where TXs adopt the harvest-then-transmit protocol, i.e., they harvest energy from the aggregate RF signal transmitted by PBs and then use the harvested energy to transmit the information to their desired RXs. Both the PT and IT phases are carried out using antenna beamforming under the mmWave channel environment, which is subjected to building blockages. Using tools from stochastic geometry, we develop a tractable analytical framework to investigate the power coverage probability, the channel coverage probability and the total coverage probability at a reference RX taking a mmWave three-state propagation model and multi-slope bounded path-loss model into account. In the proposed framework, the power coverage probability is efficiently and accurately computed by numerical inversion using the closed-form expression for the Laplace transform of the aggregate received power[1] at the typical TX. The novel contributions of this paper are summarized as follows:

- We adopt a realistic model of wirelessly powered TXs by taking into consideration (i) the power circuit activation threshold, which accounts for the minimum aggregate received power required to activate the energy harvesting circuit, (ii) the allowed maximum harvested power, which accounts for the saturation of the energy harvesting circuit and (iii) the maximum transmit power, which accounts for the safety regulation and the electrical rating of the antenna circuit.
- For tractable analysis of the channel coverage probability and the total coverage probability, we propose to discretize the transmit power of each TX into a finite number of discrete power levels in the log scale. Using this approximation, we derive the channel coverage probability and the total coverage probability at the typical RX. Comparison with simulation results shows that the model, with only 10 discrete levels for the transmit power of TXs, has good accuracy in the range of 5%-10%.
- Based on our proposed model, we investigate the impact of varying important system parameters (e.g., PB transmit power, PB density, allowed maximum harvested power, directional beamforming parameters etc.) on the network performance. These trends are summarized in Table V.
- We investigate the feasibility of using PBs to power up TXs while providing an acceptable performance for IT towards RXs in mmWave ad hoc network. Our results show that under practical setups, for PB transmit power of 50 dBm and TXs with a maximum transmit power between $20-40$ dBm, which are safe for human exposure, the total coverage probability is around 90%.

C. Notation and Paper Organization

The following notation is used in this paper. $\Pr(\cdot)$ indicates the probability measure and $\mathbb{E}[\cdot]$ denotes the expectation operator. j is the imaginary number and $\mathrm{Re}[\cdot]$ denotes the real part of a complex number. $\Gamma(x) = \int_0^\infty t^{x-1}\exp(-t)dt$ is the complete gamma function and $\Gamma(a,x) = \int_x^\infty t^{a-1}\exp(-t)dt$ is the upper incomplete gamma function, respectively. ${}_2F_1(a,b;c;z) = \frac{\Gamma(c)}{\Gamma(b)\Gamma(c-b)}\int_0^1 \frac{t^{b-1}(1-t)^{c-b-1}}{(1-tz)^a}dt$ is the Gaussian hypergeometric function. $f_X(x)$ and $F_X(x)$ denotes the probability density function (PDF) and the cumulative distribution function (CDF) of a random variable X. $\mathcal{L}_X(s) = \mathbb{E}[\exp(-sX)]$ denotes the Laplace transform of a random variable X. A list of the main mathematical symbols employed in this paper is given in Table I.

The rest of the paper is organized as follows: Section II describes the system model and assumptions. Section III focuses on the PT phase of the system and derives the power coverage probability. Section IV details the IT phase, which covers the analysis of transmit power statistics and channel coverage probability. Section V summaries the total coverage probability. Section VI presents the results and the effect of

[1] In this paper, we use the Laplace transform of a random variable to denote the Laplace transform of the distribution of a random variable for brevity.

TABLE I
SUMMARY OF MAIN SYMBOLS USED IN THE PAPER

Symbol	Definition
ϕ_p	PB PPP
ϕ_t	TX PPP
ϕ_t^n	nth level TX PPP
λ_p	Density of PB PPP
λ_t	Density of TX PPP
λ_t^n	Density of nth level TX PPP
d_0	Length of desired TX-RX link
$r_{\min}$	Radius of the LOS region
$r_{\max}$	Exclusion radius of the OUT region
α_{L}	LOS link path-loss exponent
α_{N}	NLOS link path-loss exponent
g_{L}	LOS link channel fading
g_{N}	NLOS link channel fading
m	Nakagami-m fading parameter
$G_p^{\max}$, $G_p^{\min}$, θ_p	PB beamforming parameters
$G_t^{\max}$, $G_t^{\min}$, θ_t	TX beamforming parameters
$G_r^{\max}$, $G_r^{\min}$, θ_r	RX beamforming parameters
P_p	PB transmit power
P_t	TX transmit power
P_t^n	nth level TX transmit power
k_n	Portion of TXs at the nth level
N	Number of battery levels
w	Step size of each battery level
σ^2	Noise power
η	Power conversion efficiency
ρ	Time switching parameter
γ_{PT}	Power circuit activation threshold
$P_1^{\max}$	Allowed maximum harvested power at active TX
$P_2^{\max}$	Maximum transmit power of active TX
γ_{TR}	SINR threshold
$\mathbb{P}_{\mathrm{cov}}^P$	Power coverage probability
$\mathbb{P}_{\mathrm{cov}}^C$	Channel coverage probability
$\mathbb{P}_{\mathrm{cov}}$	Total coverage probability

the system parameters on the network performance. Finally, Section VII concludes the paper.

II. SYSTEM MODEL

We consider a two-dimensional mmWave wireless ad hoc network, where TXs are first wirelessly charged by PBs and then they transmit information to RXs. The locations of PBs are modeled as a homogeneous Poisson point process (PPP) ϕ_p in $\mathbb{R}^2$ with constant node density λ_p. TXs are assumed to be randomly independently deployed and their locations are modeled as a homogeneous PPP ϕ_t with node density λ_t. For each TX, it has a desired RX located at a distance d_0 in a random direction. Throughout the paper, we use X_i to denote both the random location as well as the ith TX itself, Y_i to denote both the location and the corresponding ith RX and Z_i to denote both the location and the ith PB, respectively. Note that we assume the indoor-to-outdoor penetration loss is high. Therefore, all the PBs, TXs and RXs can be regarded as outdoor devices.

A. Power Transfer and Information Transmission Model

We assume that each PB has access to a dedicated power supply (e.g., a battery or power grid) and transmits with a constant power P_p. Time is divided into slots and T denotes one time slot. TXs adopt the harvest-then-transmit protocol to perform PT and IT. Specifically, each time slot T is divided into two parts with ratio $\rho \in (0, 1)$: in the first ρT seconds each TX harvests energy from the RF signal transmitted by PBs and stores the energy in an ideal (infinite capacity) battery.[2] In the remaining $(1-\rho)T$ seconds, TXs use all the harvested energy to transmit information to their desired RXs. Hence, there is no interference between the PT and IT stages. We make the following assumptions for realistic modelling of PT:

- Different from previous works [10], [21], [24], where energy harvesting activation threshold is not considered and the devices can harvest power from any amount of incident power, we assume that the TX can scavenge energy if and only if the instantaneous aggregate received power from all PBs is greater than a power circuit activation threshold γ_{PT}. If this condition is met, then the TX is called an *active TX*. Otherwise, the TX will be inactive and will not scavenge any energy from the PBs.
- Once the energy harvesting circuit is activated, the harvested power at the active TX is assumed to be linearly proportional to the aggregate received power with power conversion efficiency η. Due to the saturation of the energy harvesting circuit, the harvested power at the active TX cannot exceed a maximum level denoted as $P_1^{\max}$ [25]. In addition, the active TX cannot transmit information with a power greater than $P_2^{\max}$ because of the safety regulation and the electrical rating of the antenna circuit [26].

B. MmWave Blockage Model

Under outdoor mmWave transmissions, each link between the PB and the TX (i.e., PB-TX link) or between the TX and the RX (i.e., TX-RX link) is susceptible to building blockages due to their high diffraction and penetration characteristics [16]. In this work, we adopt the state-of-the-art three-state blockage model as in [17] and [27], where each PB-TX or TX-RX link can be in one of the following three states: (i) the link is in LOS state if no blockage exists, (ii) the link is in NLOS state if blockage exists and (iii) the link is in outage (OUT) state if the link is too weak to be established.

Given that the PB-TX or TX-RX link has a length of r, the probabilities $p_{\mathrm{LOS}}(\cdot)$, $p_{\mathrm{NLOS}}(\cdot)$ and $p_{\mathrm{OUT}}(\cdot)$ of it being in LOS, NLOS and OUT states, respectively, are

$$\begin{aligned} p_{\mathrm{OUT}}(r) &= u(r - r_{\max}); \\ p_{\mathrm{NLOS}}(r) &= u(r - r_{\min}) - u(r - r_{\max}); \\ p_{\mathrm{LOS}}(r) &= 1 - u(r - r_{\min}), \end{aligned} \tag{1}$$

where $u(\cdot)$ denotes the unit step function, $r_{\min}$ is the radius of the LOS region and $r_{\max}$ is the exclusion radius of the OUT region,[3] as illustrated in Fig. 1. The values of $r_{\min}$ and $r_{\max}$ depend on the propagation scenario and the mmWave carrier frequency [17]. Moreover, the communication link between TX and its desired RX is assumed to be always in LOS state.

[2] In this work, we do not consider the impact of battery imperfections [23].

[3] Note that the two-state blockage model in [28] and [29], which does not consider the OUT region, can be considered as a special case of the three-state blockage model with $r_{\max} = \infty$.

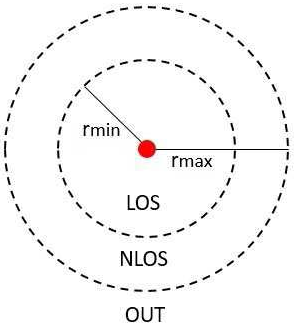

Fig. 1. Illustration of mmWave blockage model.

C. MmWave Channel Model

It has been shown by the measurements that mmWave links experience different channel conditions under LOS, NLOS and OUT states [30]. Thus, we consider the following path-loss plus block fading channel model.

For the path-loss, we adopt and modify a multi-slope path-loss model [31] and define the path-loss of PB-TX or TX-RX link with a propagation distance of r as follows

$$l(r) = \begin{cases} 1, & 0 \leqslant r < 1 \\ r^{-\alpha_{\mathrm{L}}}, & 1 \leqslant r < r_{\min} \\ \beta r^{-\alpha_{\mathrm{N}}}, & r_{\min} \leqslant r < r_{\max} \\ \infty, & r_{\max} \leqslant r \end{cases}, \tag{2}$$

where the first condition is added to avoid the singularity as $r \to 0$, α_{L} denotes the path-loss exponent for the link in LOS state, α_{N} denotes the path-loss exponent for the link in NLOS state ($2 \leqslant \alpha_{\mathrm{L}} \leqslant \alpha_{\mathrm{N}}$), the path-loss of the link in OUT state is assumed to be infinite [17] and the continuity in the multi-slope path-loss model is maintained by introducing the constant $\beta \triangleq r_{\min}^{\alpha_{\mathrm{N}}-\alpha_{\mathrm{L}}}$ [31].

As for the fading, the link under LOS state is assumed to experience Nakagami-m fading, while the link under NLOS state is assumed to experience Rayleigh fading.[4] Furthermore, both the LOS and the NLOS links experience additive white Gaussian noise (AWGN) with variance σ^2. However, under the PT phase, the AWGN power is too small to be harvested by TXs. Hence, we ignore it in the PT phase.

D. Beamforming Model

To compensate the large path-loss in mmWave band, directional beamforming is necessary for devices [33]. In this work, we consider that mmWave antenna arrays perform directional beamforming at all PBs, TXs and RXs. Similar to [16] and [17], the actual antenna array pattern can be approximated by a sectorized gain pattern which is given by

$$G_a(\theta) = \begin{cases} G_a^{\max}, & |\theta| \leq \dfrac{\theta_a}{2} \\ G_a^{\min}, & \text{otherwise} \end{cases}, \tag{3}$$

where subscript $a = p$ for PB, $a = t$ for TX and $a = r$ for RX, $G_a^{\max}$ is the main lobe antenna gain, $G_a^{\min}$ is the side lobe antenna gain, $\theta \in [-\pi, \pi)$ is the angle off the boresight direction and θ_a is the main lobe beam-width. Note that, as shown in Section VI-C, this model can be easily related to specific array geometries, such as an N element uniform planar or linear or circular array [18].

[4]We do not consider shadowing but it can be included using the composite fading model in [32].

TABLE II
PROBABILITY MASS FUNCTION OF G_{ij} AND D_{ij}.

	PB-TX gain G_{ij}		TX-RX gain D_{ij}	
k	Gain G_k	Probability p_k	Gain D_k	Probability q_k
1	$G_p^{\max}G_t^{\max}$	$\frac{\theta_p\theta_t}{4\pi^2}$	$G_t^{\max}G_r^{\max}$	$\frac{\theta_t\theta_r}{4\pi^2}$
2	$G_p^{\max}G_t^{\min}$	$\frac{\theta_p(2\pi-\theta_t)}{4\pi^2}$	$G_t^{\max}G_r^{\min}$	$\frac{\theta_t(2\pi-\theta_r)}{4\pi^2}$
3	$G_p^{\min}G_t^{\max}$	$\frac{(2\pi-\theta_p)\theta_t}{4\pi^2}$	$G_t^{\min}G_r^{\max}$	$\frac{(2\pi-\theta_t)\theta_r}{4\pi^2}$
4	$G_p^{\min}G_t^{\min}$	$\frac{(2\pi-\theta_p)(2\pi-\theta_t)}{4\pi^2}$	$G_t^{\min}G_r^{\min}$	$\frac{(2\pi-\theta_t)(2\pi-\theta_r)}{4\pi^2}$

The main beam at the PBs are assumed to be randomly and independently oriented with respect to each other and uniformly distributed in $[-\pi, \pi)$. Given a sufficient density of the PBs, this simple strategy ensures that the aggregate received power from PBs at different locations in the network is roughly on the same order and avoids the need for channel estimation and accurate beam alignment. In addition, it has been shown in [33] that the random directional beamforming can perform reasonably well given that more than one users need to be served.

Let G_{ij} be the effective antenna gain on the link from the ith PB to the jth TX. Under sectorization, G_{ij} is a discrete random variable with probability $p_k = \Pr(G_{ij} = G_k)$ and $k \in \{1, 2, 3, 4\}$, where its distribution is summarized in Table II.

With regards to TX and RX, we assume that each TX points its main lobe towards its desired RX directly. Therefore, the effective antenna gain of the desired TX-RX link is $D_0 = G_t^{\max}G_r^{\max}$ and the orientation of the beam of the interfering TX is uniformly distributed in $[-\pi, \pi)$. Let $D_{ij} (i \neq j)$ be the effective antenna gain on the link from the ith TX to the jth RX. Similar to G_{ij}, D_{ij} is a discrete random variable with probability $q_k = \Pr(D_{ij} = D_k)$, where its distribution is given in Table II.

E. Metrics

In this paper, we are interested in the PB-assisted mmWave wireless ad hoc network in terms of the total coverage probability for RXs (i.e., the probability that a RX can successfully receive the information from its TX after the TX successfully harvests energy from PBs). Based on the system model described above, the success of this event has to satisfy two requirements, which are:

- *The corresponding TX is in power coverage*. Due to the random network topology and the fading channels, the aggregate received power from all PBs is a random variable. If the aggregate received power at a TX is greater than the power circuit activation threshold, the energy harvesting circuit is active and this TX can successfully harvest energy from PBs. As a result, the TX is under power coverage and IT then takes place.

- *The RX is in channel coverage*. The instantaneous transmit power for each active TX depends on its random received power. RX can receive the information from its desired TX (i.e., in channel coverage) if the signal-to-interference-plus-noise ratio (SINR) at the RX is above a certain threshold.

By leveraging the Laplace transform of the aggregate received power at a typical TX and the interference at a typical RX, we compute the power coverage probability and channel coverage probability in the following sections. In the subsequent analysis, we condition on having a reference RX Y_0 at the origin $(0,0)$ and its associated TX X_0 located at a distance d_0 away at $(d_0,0)$. According to Slivnyak's theorem, the conditional distribution is the same as the original one for the rest of the network [34].

III. Power Transfer

In this section, we focus on the PT phase of the system. We analyze the aggregate received power at a reference TX from all PBs and find the power coverage probability at the corresponding RX.

Since the power harvested from the noise is negligible, the instantaneous aggregate received power at the typical TX X_0 from all the PBs can be expressed as

$$P_{\mathrm{PT}} = P_p \sum_{Z_i \in \phi_p} G_{i0} g_{i0} l(r_i), \tag{4}$$

where P_p is the PB transmit power, G_{i0} is the effective antenna gain between Z_i and X_0, g_{i0} is the fading power gain between the ith PB Z_i and the typical TX X_0, which follows the gamma distribution (under Nakagami-m fading assumption) if the PB-TX link is in LOS state and exponential distribution (under Rayleigh fading distribution) if the PB-TX link is in NLOS state. $l(r_i)$ is the path-loss function given in (2) and $r_i = |Z_i - X_0|$ is the Euclidean length of the PB-TX link between Z_i and X_0. Using (4), the power coverage probability is defined as follows.

Definition 1: The power coverage probability is the probability that the aggregate received power at the typical TX is higher than the power circuit activation threshold γ_{PT}. It can be expressed as

$$\mathbb{P}^{P}_{\mathrm{cov}}(\gamma_{\mathrm{PT}}) = \Pr(P_{\mathrm{PT}} > \gamma_{\mathrm{PT}}). \tag{5}$$

Remark 1: Analytically characterizing the power coverage probability in (5) is a challenging open problem in the literature. Generally, it is not possible to obtain a closed-form power coverage probability because of the randomness in the antenna gain, mmWave channels and locations of PBs. The closed-form expression only exists under the unbounded path-loss model with $\alpha = 4$ and Rayleigh fading for all links, which is shown to be Lévy distribution [34]. To overcome this problem, some works [20], [28], [35] employed the Gamma scaling method. This approach involves introducing a dummy Gamma random variable with parameter N' to reformulate the original problem. However, the approach can sometimes lead to large errors with finite N' value. Other works adopted the Gil-Pelaez inversion theorem [36]. This approach involves one fold integration and is only suitable for the random variable with a simple Laplace transform. If the Laplace transform is even moderately complicated, this method is not very efficient even if the Laplace transform is in closed-form.

In this work, we adopt a numerical inversion method, which is easy to compute, if the Laplace transform of a random variable is in closed-form, and provides controllable error estimation. Following [37] and [38], the CDF of the aggregate received power P_{PT} is given as

$$F_{P_{\mathrm{PT}}}(x) = \frac{1}{2\pi j}\int_{a-j\infty}^{a+j\infty} \mathcal{L}_{F_{P_{\mathrm{PT}}}}(s)\exp(sx)ds \tag{6a}$$

$$= \frac{1}{2\pi j}\int_{a-j\infty}^{a+j\infty} \frac{\mathcal{L}_{P_{\mathrm{PT}}}(s)}{s}\exp(sx)ds. \tag{6b}$$

where (6a) is obtained according to the Bromwich integral [39] and (6b) follows from probability theory that $\mathcal{L}_{P_{\mathrm{PT}}}(s) = s\mathcal{L}_{F_{P_{\mathrm{PT}}}}(s)$. Using the trapezoidal rule and the Euler summation, the above integral can be transformed into a finite sum. Therefore, we can express the power coverage probability as

$$\mathbb{P}^{P}_{\mathrm{cov}}(\gamma_{\mathrm{PT}}) = 1 - \frac{2^{-B}\exp(\frac{A}{2})}{\gamma_{\mathrm{PT}}}\sum_{b=0}^{B}\binom{B}{b} \times \sum_{c=0}^{C+b}\frac{(-1)^c}{D_c}\mathrm{Re}\left[\frac{\mathcal{L}_{P_{\mathrm{PT}}}(s)}{s}\right], \tag{7}$$

where $\mathrm{Re}[\cdot]$ is the real part operator, $s = \frac{A+j2\pi c}{2\gamma_{\mathrm{PT}}}$, $\mathcal{L}_{P_{\mathrm{PT}}}(s)$ is the Laplace transform of P_{PT}, $D_c = 2$ (if $c = 0$) and $D_c = 1$ (if $c = 1, 2, \ldots, C+b$). A, B and C are positive parameters used to control the estimation accuracy.

From (7), the key parameter in order to obtain the power coverage probability is $\mathcal{L}_{P_{\mathrm{PT}}}(s)$. By the definition of Laplace transform of a random variable, we express $\mathcal{L}_{P_{\mathrm{PT}}}(s)$ in closed-form in the following theorem.

Theorem 1: Following the system model in Section II, the Laplace transform of the aggregate received power at the typical TX from all the PBs in a mmWave ad hoc network is

$$\begin{aligned}\mathcal{L}_{P_{\mathrm{PT}}}(s) &= \prod_{k=1}^{4}\exp\Big(\pi\lambda_p r_{\min}^2 p_k\Big(m^m(m+sr_{\min}^{-\alpha_{\mathrm{L}}}P_pG_k)^{-m}-1\Big) \\ &\quad + \pi\lambda_p p_k\left(sP_pG_k\right)^{\delta_{\mathrm{L}}}\left(\Xi_1(1)-\Xi_1(r_{\min})\right) \\ &\quad + \pi\lambda_p p_k sP_pG_k\beta\left(\Xi_2(r_{\min})-\Xi_2(r_{\max})\right) \\ &\quad + \frac{\pi\lambda_p}{2+\alpha_{\mathrm{N}}}p_k(sP_pG_k\beta)^{\delta_{\mathrm{N}}}(\Xi_3(r_{\min})-\Xi_3(r_{\max}))\Big),\end{aligned} \tag{8}$$

where

$$\Xi_1(r) = \frac{m^m(r^{-\alpha_{\mathrm{L}}}sP_pG_k)^{-\delta_{\mathrm{L}}-m}\alpha_{\mathrm{L}}\Gamma(1+m)}{(2+m\alpha_{\mathrm{L}})\Gamma(m)} \times {}_2F_1\left(1+m, m+\delta_{\mathrm{L}}; 1+m+\delta_{\mathrm{L}}; -\frac{mr^{\alpha_{\mathrm{L}}}}{sP_pG_k}\right), \tag{9}$$

$$\Xi_2(r) = \frac{r^2}{r^{\alpha_{\mathrm{N}}}+sP_pG_k\beta}, \tag{10}$$

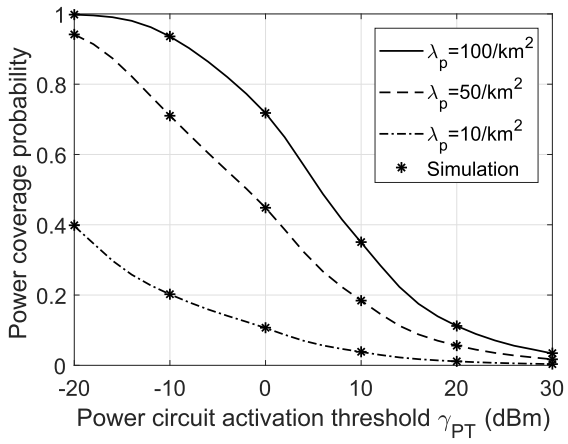

Fig. 2. Power coverage probability versus power circuit activation threshold γ_{PT} for different PB densities. Other system parameters follow Table IV.

$$\Xi_3(r) = \frac{(r^{-\alpha_{\mathrm{N}}} s P_p G_k \beta)^{-\delta_{\mathrm{N}}-1}}{r^{\alpha_{\mathrm{N}}} + s P_p G_k \beta} \times \left(s P_p G_k \beta (2+\alpha_{\mathrm{N}}) - 2(r^{\alpha_{\mathrm{N}}} + s P_p G_k \beta) \times {}_2F_1\left(1, \delta_{\mathrm{N}}+1; 2+\delta_{\mathrm{N}}; -\frac{r^{\alpha_{\mathrm{N}}}\beta^{-1}}{s P_p G_k}\right)\right), \quad (11)$$

and $\Gamma(\cdot)$ is the complete gamma function, ${}_2F_1(\cdot,\cdot;\cdot;\cdot)$ is the Gaussian (or ordinary) hypergeometric function, $\delta_{\mathrm{L}} \triangleq \frac{2}{\alpha_{\mathrm{L}}}$ and $\delta_{\mathrm{N}} \triangleq \frac{2}{\alpha_{\mathrm{N}}}$.

Proof: See Appendix A. ∎

By substituting (8) into (7), we can compute the power coverage probability. As shown in Theorem 1, the Laplace transform of P_{PT} is in closed-form; hence, $\mathbb{P}^{P}_{\mathrm{cov}}(\gamma_{\mathrm{PT}})$ is just a summation over a finite number of terms. Following the selection guideline of parameters A, B and C in [38], we can achieve a stable numerical result by carefully choosing them.

Finally, we validate the analysis for the power coverage probability. Fig. 2 plots the power coverage probability versus power circuit activation threshold. The simulation results are generated by averaging over 10^8 Monte Carlo simulation runs. We set $A = 24$, $B = 20$ and $C = 30$ in order to achieve an estimation error of 10^{-10}. The other system parameters follow Table IV. From the figure, we can see that the analytical results match perfectly with the simulation results, which demonstrates the accuracy of the proposed approach. Fig. 2 also shows that the power coverage probability increases with the density of PBs, because the aggregate received power at TX increases as the PB density increases.

IV. Information Transmission

In this section we focus on the IT phase between the TX and RX. We assume that the TX uses all the harvested energy in the IT phase. As indicated in Section II-A, the transmit power of an active TX is a random variable which depends on its harvested power. Hence, we first evaluate the transmit power for an active TX. Then, we calculate the channel coverage probability at the reference RX. Note that the derived channel coverage probability is in fact a conditional probability, which is conditioned on the reference TX-RX link being active.

A. Transmit Power and Locations of Active TX

Using the PT assumptions in Section II-A, the instantaneous transmit power for each active TX is

$$P_t = \begin{cases} \frac{\eta\rho}{1-\rho} P_{\mathrm{PT}}, \\ \quad \min(\frac{P_1^{\max}}{\eta}, \frac{1-\rho}{\eta\rho} P_2^{\max}) > P_{\mathrm{PT}} \geqslant \gamma_{\mathrm{PT}} \\ \min(\frac{\rho P_1^{\max}}{1-\rho}, P_2^{\max}), \\ \quad P_{\mathrm{PT}} \geqslant \min(\frac{P_1^{\max}}{\eta}, \frac{1-\rho}{\eta\rho} P_2^{\max}), \end{cases} \quad (12)$$

where $0 \leqslant \eta \leqslant 1$ is the power conversion efficiency. Note that the first condition in (12) comes from the fact that the received power at an active TX must be greater than γ_{PT}. For the second condition in (12), $P_1^{\max}$ is the maximum harvested power at an active TX when the energy harvesting circuit is saturated and $P_2^{\max}$ is the maximum transmit power for an active TX. Thus, the second condition caps the transmit power by the allowed maximum harvested power constraint or the maximum transmit power constraint.

The following remarks discuss the modelling challenges and proposed solution for characterizing P_t.

Remark 2: To the best of our knowledge, the closed-form expression for the PDF of P_t is very difficult to obtain. This is because P_t and P_{PT} are correlated and the closed-form CDF of P_{PT} is not available according to Section III. In the literature, some papers [21], [40] have proposed to use the average harvested power as the transmit power for each TX. However, this does not always lead to accurate results. Hence, inspired from the approach in [41], we propose to discretize P_t in (12) into a finite number of levels. We show that this approximation allows tractable computation of the channel coverage probability. The accuracy of this approximation depends on the number of levels. Our results in Section VI-A show that if we discretize the power level in the log scale, a reasonable level of accuracy is reached with as little as 10 levels.

Remark 3: From (12), we can see that P_t depends on P_{PT}. Hence, the motivation for discretizing P_t in the log scale comes from looking into two important measures of P_{PT}, the skewness and the kurtosis. The skewness and the kurtosis describe the shape of the probability distribution of P_{PT}. As presented in [22], the distribution of the aggregate received power is skewed to the right with a heavy tail, because both the skewness and the kurtosis of P_{PT} are much greater than 0 for most cases. Therefore, most of the TXs will be at the lowest power level if we discretize P_t in linear scale. Hence, we discretize the power level in the log scale. This improves the accuracy of the approximation.

Let $N+1$ and w denote the total number of levels and the step size of each level, respectively. They are related by $w = \left(\frac{\min\left(\eta^{-1}P_1^{\max}, \frac{1-\rho}{\eta\rho}P_2^{\max}\right) - \gamma_{\mathrm{PT}}}{N}\right)$dBm. We further define k_n as the portion of TXs whose P_t is at the nth level, i.e., $k_n = \Pr\left((nw+\gamma_{\mathrm{PT}})\,\mathrm{dBm} \leqslant P_{\mathrm{PT}} < ((n+1)w+\gamma_{\mathrm{PT}})\,\mathrm{dBm}\right)$ for $n = \{0,1,2,\ldots,N-1\}$ and $k_N = \Pr(P_{\mathrm{PT}} \geqslant \min(\eta^{-1}P_1^{\max}, \frac{1-\rho}{\eta\rho}P_2^{\max}))$. Combining with the power coverage probability derived in Section III, we can

express k_n as

$$k_n=\begin{cases}\mathbb{P}^P_{\text{cov}}((n w+\gamma_{\text{PT}})\text{dBm})\\ -\mathbb{P}^P_{\text{cov}}(((n+1)\, w+\gamma_{\text{PT}})\,\text{dBm}),\\ \qquad\qquad n=\{0,1,2,\ldots,N-1\}\\ \mathbb{P}^P_{\text{cov}}\left(\min\left(\frac{P_1^{\max}}{\eta},\frac{1-\rho}{\eta\rho}P_2^{\max}\right)\right),\\ \qquad\qquad n=N.\end{cases} \tag{13}$$

The above expression allows us to determine the portion of TXs whose P_t is at the nth level. The transmit power for the active TX at the nth level is

$$P_t^n=\left(\eta\frac{\rho}{1-\rho}10^{\frac{n w+\gamma_{\text{PT}}-30}{10}}\right)\text{W}. \tag{14}$$

The next step is to decide how to model the locations of the TXs whose P_t is at the nth level. This is discussed in the remark below.

Remark 4: In general, the location and the transmit power of an active TX are correlated, i.e., a TX has higher chance to be activated and transmits with a larger power, if its location is closer to a PB. However, it is not easy to identify and fit a spatial point process with local clustering to model the location of active TXs [14], [42]. In this paper, for analytical tractability, we assume that the location and the transmit power of an active TX are independent, i.e., a TX in ϕ_t can have a transmit power of P_t^n with probability k_n independently of other TXs. Therefore, using the thinning theorem, we interpret the active TX at the nth level as an independent homogeneous PPP with node density $\lambda_t^n=k_n\lambda_t$, denoted as ϕ_t^n. The accuracy of this approximation will be validated in Section VI-A.

B. Channel Coverage Probability

Given that the desired TX is active, the instantaneous SINR at the reference RX, Y_0, is given as

$$SINR=\frac{P_{X_0}D_0h_0l(d_0)}{\sum_{X_i\in\phi_{\text{active}}}P_{X_i}D_{i0}h_{i0}l(X_i)+\sigma^2}, \tag{15}$$

where h_0 and h_{i0} denote the fading power gains on the reference link and the ith interference link respectively, D_0 and D_{i0} denote the beamforming antenna gain at the RX from its reference TX and the ith interfering TX respectively and σ^2 is the AWGN power. P_{X_0} and P_{X_i} are the transmit power for the reference TX and the active TX X_i, respectively. Using (15), the power coverage probability is defined as follows.

Definition 2: The channel coverage probability is the probability that the SINR at the reference RX is above a threshold γ_{TR} and can be expressed as

$$\mathbb{P}^C_{\text{cov}}(\gamma_{\text{TR}})=\Pr(SINR>\gamma_{\text{TR}}). \tag{16}$$

Remark 5: It is possible to employ the numerical inversion method in Section III to find the channel coverage probability. In doing so, the Laplace transform of the term $\frac{I_X+\sigma^2}{P_{X_0}D_0\ h_0\ l(d_0)}$ is required. This Laplace tranform cannot be expressed in closed-form because of the random variables P_{X_0} and h_0 in the denominator. Although it is still computable, it leads to greater computation complexity. Consequently, we employ the reference link power gain (RLPG) based method in [38] to efficiently find the channel coverage probability. The basic principle of this approach is to first find the conditional outage probability in terms of the CDF of the reference links fading power gain and then remove the conditioning on the fading power gains and locations of the interferers, respectively. In order to apply this method, the reference TX-RX link is assumed to undergo Nakagami-m fading with integer m. The result for the conditional channel coverage probability is presented in the following proposition.

Proposition 1: Following the system model in Section II, the conditional channel coverage probability at the reference RX in a mmWave ad hoc network is

$$\mathbb{P}^C_{\text{cov}}(\gamma_{\text{TR}})=\sum_{n=0}^{N}\sum_{l=0}^{m-1}\frac{(-s)^l}{l!}\frac{dl}{ds^l}\mathcal{L}_{I_X+\sigma^2}(s)\frac{k_n}{\mathbb{P}^P_{\text{cov}}(\gamma_{\text{PT}})}, \tag{17}$$

where $I_X=\sum_{n=0}^{N}\sum_{X_i\in\phi_t^n}P_t^nD_{i0}h_{i0}l(X_i)$ and $s=\frac{m\gamma_{\text{TR}}}{P_t^nD_0l(d_0)}$.

Proof: See Appendix B. ∎

(17) needs the Laplace transform of the interference plus noise. Using stochastic geometry, we can derive it and the result is shown in the following corollary.

Corollary 1: Following the system model in Section II and the discretization assumption in Section IV-A, the Laplace transform of the aggregate interference plus noise at the reference RX in a mmWave ad hoc network is

$$\begin{aligned}&\mathcal{L}_{I_X+\sigma^2}(s)\\ &=\prod_{n=0}^{N}\prod_{k=1}^{4}\exp\Big(\pi\lambda_t^nr_{\min}^2q_k\left(m^m(m+sr_{\min}^{-\alpha_{\text{L}}}P_t^nD_k)^{-m}-1\right)\\ &\quad+\pi\lambda_t^nq_k\left(sP_t^nD_k\right)^{\delta_{\text{L}}}\left(\Xi_1'(1)-\Xi_1'(r_{\min})\right)\\ &\quad+\pi\lambda_t^nq_ksP_t^nD_k\beta\left(\Xi_2'(r_{\min})-\Xi_2'(r_{\max})\right)+\frac{\pi\lambda_t^n}{2+\alpha_{\text{N}}}q_k\\ &\quad\times(sP_t^nD_k\beta)^{\delta_{\text{N}}}\left(\Xi_3'(r_{\min})-\Xi_3'(r_{\max})\right)\Big)\exp(-s\sigma^2),\end{aligned} \tag{18}$$

where

$$\begin{aligned}\Xi_1'(r)&=\frac{m^m(r^{-\alpha_{\text{L}}}sP_t^nD_k)^{-\delta_{\text{L}}-m}\alpha_{\text{L}}\Gamma(1+m)}{(2+m\alpha_{\text{L}})\Gamma(m)}\\ &\quad\times{}_2F_1\left(1+m,m+\delta_{\text{L}};1+m+\delta_{\text{L}};-\frac{mr^{\alpha_{\text{L}}}}{sP_t^nD_k}\right),\end{aligned} \tag{19}$$

$$\Xi_2'(r)=\frac{r^2}{r^{\alpha_{\text{N}}}+sP_t^nD_k\beta}, \tag{20}$$

$$\begin{aligned}\Xi_3'(r)&=\frac{(r^{-\alpha_{\text{N}}}sP_t^nD_k\beta)^{-\delta_{\text{N}}-1}}{r^{\alpha_{\text{N}}}+sP_t^nD_k\beta}\\ &\quad\times\Big(sP_t^nD_k\beta(2+\alpha_{\text{N}})-2(r^{\alpha_{\text{N}}}+sP_t^nD_k\beta)\\ &\quad\times{}_2F_1\left(1,\delta_{\text{N}}+1;2+\delta_{\text{N}};-\frac{r^{\alpha_{\text{N}}}\beta^{-1}}{sP_t^nD_k}\right)\Big).\end{aligned} \tag{21}$$

Proof: Following the definition of Laplace, transform, we have

$$\begin{aligned}\mathcal{L}_{I_X+\sigma^2}(s)&=\mathbb{E}_{I_X}[\exp(-s(I_X+\sigma^2))]\\ &=\mathbb{E}_{I_X}[\exp(-sI_X)]\exp(-s\sigma^2)\\ &=\mathcal{L}_{I_X}(s)\exp(-s\sigma^2),\end{aligned} \tag{22}$$

TABLE III

SUMMARY OF THE ANALYTICAL MODEL FOR PB-ASSISTED MMWAVE AD HOC NETWORKS

Performance metrics	General form	Key factor(s)
Power coverage probability	(7)	$\mathcal{L}_{P_{\mathrm{PT}}}(s)$ in (8)
Channel coverage probability	(17)	$\mathbb{P}^{P}_{\mathrm{cov}}(\gamma_{\mathrm{PT}})$ in (7) $\mathcal{L}_{I_X+\sigma^2}(s)$ in (18)
Total coverage probability	(24)	$\mathbb{P}^{P}_{\mathrm{cov}}(\gamma_{\mathrm{PT}})$ in (7) $\mathcal{L}_{I_X+\sigma^2}(s)$ in (18)

where the Laplace transform of the aggregate interference can be expressed as

$$\begin{aligned}
&\mathcal{L}_{I_X}(s)\\
&= \mathbb{E}_{I_X}[\exp(-sI_X)]\\
&= \mathbb{E}_{D_{i0},h_{i0},\phi_t^n}\left[\exp\left(-s\sum_{n=0}^{N}\sum_{X_i\in\phi_t^n} P_t^n D_{i0}h_{i0}l(X_i)\right)\right]\\
&= \prod_{n=0}^{N}\mathbb{E}_{D_{i0},h_{i0},\phi_t^n}\left[\exp\left(-s\sum_{X_i\in\phi_t^n} P_t^n D_{i0}h_{i0}l(X_i)\right)\right]. \quad (23)
\end{aligned}$$

Then, following the same steps as the proof of Laplace transform of aggregate received power in Appendix A, we can find the expectation in (23) and arrive at the result in (18). ■

The Laplace transform shown in Corollary 1 is in closed-form. Substituting (18) into (17), we can easily compute the conditional channel coverage probability. Note that (17) requires higher order derivatives of the Laplace transform of the interference plus noise $\frac{dl}{ds^l}\mathcal{L}_{I_X+\sigma^2}(s)$, which can be yielded in closed-form using chain rules and changing variables. For brevity, the details are omitted here.

V. TOTAL COVERAGE PROBABILITY

As discussed in Section II-E, the event that the information can be successfully delivered to RX has two requirements, i.e., satisfying power coverage and channel coverage. Based on our definition, the total coverage probability is

$$\begin{aligned}
&\mathbb{P}_{\mathrm{cov}}(\gamma_{\mathrm{PT}},\gamma_{\mathrm{TR}})\\
&= \Pr(\text{TX is in power coverage \& RX is in channel coverage})\\
&= \Pr(\text{TX is in power coverage})\\
&\times \Pr(\text{RX is in channel coverage} \mid \text{TX is in power coverage})
\end{aligned}$$

Combining our analysis presented in Section III and IV, we have

$$\begin{aligned}
\mathbb{P}_{\mathrm{cov}}(\gamma_{\mathrm{PT}},\gamma_{\mathrm{TR}}) &= \mathbb{P}^{P}_{\mathrm{cov}}(\gamma_{\mathrm{PT}})\mathbb{P}^{C}_{\mathrm{cov}}(\gamma_{\mathrm{TR}})\\
&= \sum_{n=0}^{N}\sum_{l=0}^{m-1}\frac{(-s)^l}{l!}\frac{dl}{ds^l}\mathcal{L}_{I_X+\sigma^2}(s)k_n, \quad (24)
\end{aligned}$$

where $s=\frac{m\gamma_{\mathrm{TR}}}{P_t^n D_0 l(d_0)}$, $\mathcal{L}_{I_X+\sigma^2}(s)$ is given in Corollary 1, k_n is presented in (13), which is determined by the power coverage probability. The key metrics are summarized in Table III.

VI. RESULTS

In this section, we first validate the proposed model and then discuss the design insights provided by the model. Unless stated otherwise, the values of the parameters summarized in Table IV are used. The chosen values are consistent with the literature in mmWave and WPT [1], [16], [17]. Note that the values of $r_{\min}$ and $r_{\max}$ correspond to 28 GHz mmWave carrier frequency [16]. We mainly focus on illustrating the results for total coverage probability and channel coverage probability. As for the power coverage probability, it will be explained within the text.

TABLE IV

PARAMETER VALUES

Parameter	Value	Parameter	Value
λ_p	50 /km^2	m	5
λ_t	100 /km^2	$G_p^{\max}$, $G_p^{\min}$, θ_p	[20 dB, -10 dB, 30°]
d_0	20 m	$G_t^{\max}$, $G_t^{\min}$, θ_t	[10 dB, -10 dB, 45°]
$r_{\min}$	100 m	$G_r^{\max}$, $G_r^{\min}$, θ_r	[10 dB, -10 dB, 45°]
$r_{\max}$	200 m	σ^2	-30 dBm
α_{L}	2	ρ	0.5
α_{N}	4	η	0.5
P_p	40 dBm	γ_{PT}	-20 dBm
$P_1^{\max}$	20 dBm	γ_{TR}	30 dBm
$P_2^{\max}$	30 dBm	N	10

TABLE V

EFFECT OF IMPORTANT SYSTEM PARAMETERS

Parameter	Power coverage	Channel coverage	Total coverage
Increasing γ_{TR}	-	$\downarrow$	$\downarrow$
Increasing λ_p	$\uparrow$	$\downarrow\uparrow$	$\uparrow$
Increasing λ_t	-	$\downarrow$	$\downarrow$
Increasing P_p	$\uparrow$	$\uparrow$	$\uparrow$
Increasing $r_{\min}$	$\uparrow$	$\uparrow$	$\uparrow$
Increasing γ_{PT}	$\downarrow$	$\uparrow$	$\downarrow$
Increasing θ_t and θ_r	$\uparrow$	$\downarrow$	$\downarrow$
Increasing $P_1^{\max}$	-	$\uparrow\downarrow$	$\uparrow\downarrow$
Increasing ρ	-	$\uparrow$	$\uparrow$
Increasing $P_2^{\max}$	-	$\downarrow$	$\downarrow$

Table V summarizes the impact of varying the important system parameters,[5] i.e., SINR threshold γ_{TR}, PB density λ_p, TX density λ_t, PB transmit power P_p, radius of the LOS region $r_{\min}$, power circuit activation threshold γ_{PT}, the beam-width of the main lobe of TX θ_t, RX's main lobe beam-width θ_r, allowed maximum harvested power at active TX $P_1^{\max}$, time switching parameter ρ and TX maximum transmit power $P_2^{\max}$ on the three network performance metrics. In Table V, $\uparrow$, $\downarrow$ and - denote increase, decrease and unrelated, respectively. $\uparrow\downarrow$ represents that the performance metric first increases then decreases with the system parameter. Please note that the trends in Table V originate from the analysis of the numerical results, which is presented in detail in the following subsections.

A. Model Validation

In this section, we validate the proposed model for the channel coverage probability and the total coverage probability. Fig. 3 plots the channel coverage probability and the total coverage probability for a reference RX against SINR threshold for different densities of PBs and TXs. The

[5]Note that the trends reported in Table V remain the same for a two-state blockage model.

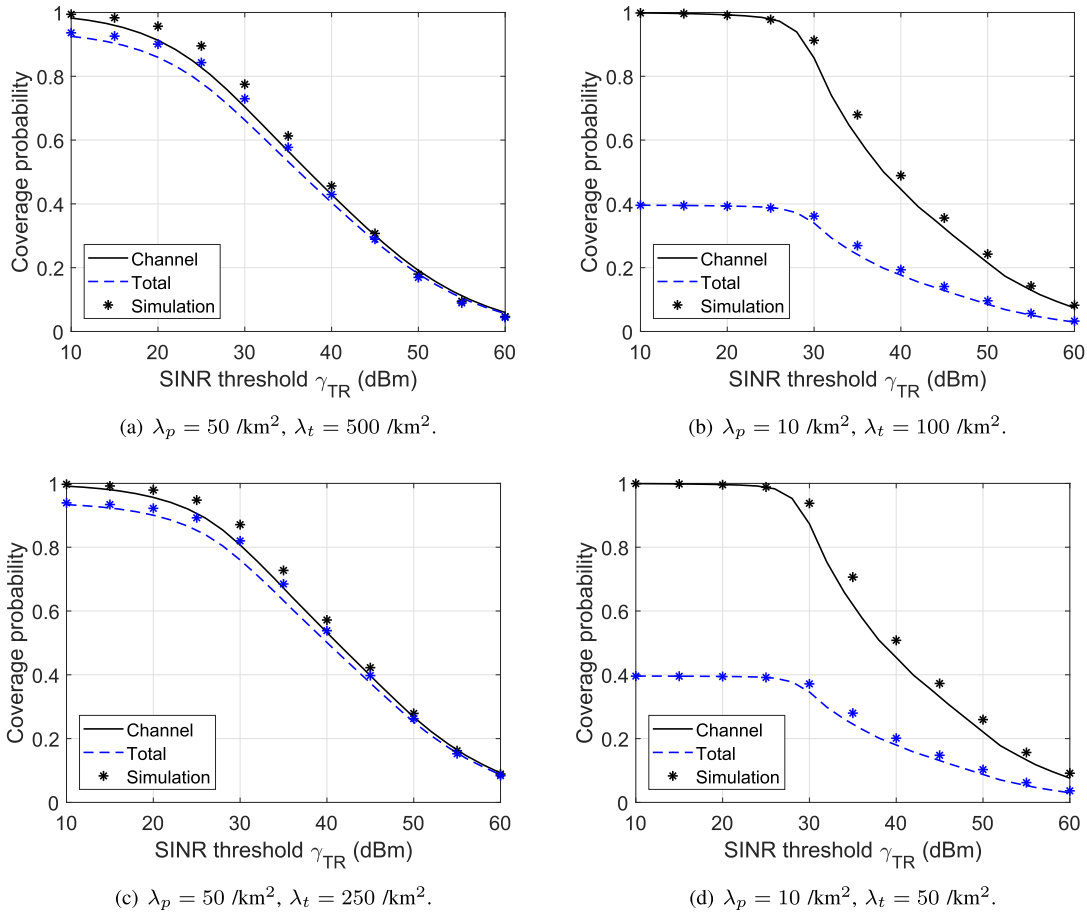

(a) $\lambda_p = 50$ /km^2, $\lambda_t = 500$ /km^2.

(b) $\lambda_p = 10$ /km^2, $\lambda_t = 100$ /km^2.

(c) $\lambda_p = 50$ /km^2, $\lambda_t = 250$ /km^2.

(d) $\lambda_p = 10$ /km^2, $\lambda_t = 50$ /km^2.

Fig. 3. Channel coverage probability and total coverage probability versus SINR threshold γ_{TR}. The PB density is 50 and 10 per km^2 and the TX density is 500, 100, 250 and 50 per km^2.

analytical results are obtained using Proposition 1 and (24) with 10 discrete levels for P_t. The simulation results are generated by averaging over 10^8 Monte Carlo simulation runs and do not assume any discretization of power levels.

From the figure, we can see that our analytical results provide a good approximation to the simulation. The small gap between them comes from two reasons: (i) discretization of the power levels, as discussed in Remark 3, and (ii) ignorance of the correlation between the location and the transmit power of active TX, as discussed in Remark 4. From Fig. 3, we can see that the gap between the simulation and the analytical results is smaller, when γ_{TR} is higher. At $\gamma_{\text{TR}} = 30$ dBm, which is a typical SINR threshold, the relative errors between the proposed model and the simulation results for both channel coverage probability and total coverage probability are between 5% to 10%. This validates the use of 10 discrete levels for P_t, which provides good accuracy.

Insights: Comparing the four cases for the different PB and TX densities, Fig. 3 shows that: (i) The channel coverage probability decreases while the total coverage probability increases as PB density increases. As the PB density increases, the aggregate received power at TX increases as well as the number of active TXs. Therefore, interfering power received by the RX is higher and the channel coverage probability decreases. However, the total coverage probability increases because the power coverage probability increases with the PB density. (ii) When the PB density is low, the TXs are very likely to be inactive and the total coverage probability is dominated by the power coverage probability. When the PB density is high, the TXs are very likely to be active. Hence, the interference is strong and the channel coverage probability dominates the total coverage probability. (iii) For the same PB density, both the total coverage probability and the channel coverage probability are higher, when the TX density is lower. This is because more interfering TXs exist if TX density increases.

B. Effect of PB Transmit Power

Fig. 4(a) illustrates the effect of PB transmit power P_p on the total coverage probability and channel coverage probability, with different radius of the LOS region $r_{\min} = 50$m, 100m. The simulation results are also plotted in the figure, which are averaged over 10^8 Monte Carlo simulation runs. The accuracy is between 3% to 8%, which again validates the proposed model. Hence, in the subsequent figures in the paper we only show the analytical results and discuss the insights.

Fig. 4(b) plots the total coverage probability against the transmit power of PB. We also plot an asymptotic result when P_p approaches infinity. This result is obtained as follows. As P_p approaches infinity, if one or more PBs fall into the

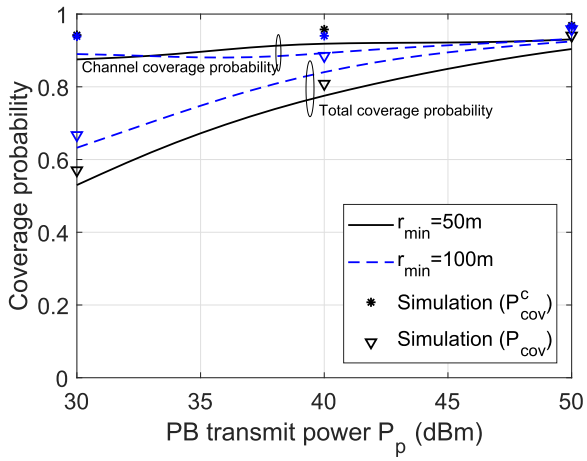

(a) Channel coverage and total coverage with different $r_{\min}$.

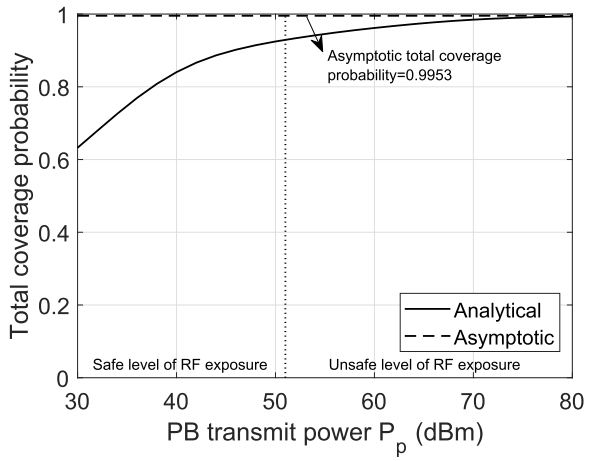

(b) Total coverage and asymptotic total coverage.

Fig. 4. Coverage probabilities versus PB transmit power P_p.

LOS or NLOS region of a TX, this TX will be active and transmit with a power of $P_t = \min(\frac{\rho}{1-\rho} P_1^{\max}, P_2^{\max})$. Hence, the asymptotic power coverage probability is equivalent to the probability that at least one PB falls into the LOS or NLOS region of the TX, which is given by

$$\lim_{P_p \to \infty} \mathbb{P}_{\text{cov}}^{P} = 1 - \exp\left(-\pi \lambda_p r_{\max}^2\right). \tag{25}$$

The asymptotic conditional channel coverage probability and the asymptotic total coverage probability can be found by (17) and (24) respectively with the portion of TXs at the nth level as

$$\lim_{P_p \to \infty} k_n = \begin{cases} 0, & n = \{0, 1, 2, \ldots, N-1\} \\ \mathbb{P}_{\text{cov}}^{P}, & n = N. \end{cases} \tag{26}$$

From the figure, we can see that the analytical and asymptotic results converge as P_p gets large, which validates the derivation of the asymptotic results. In addition, in Fig. 4(b), we have marked the safe RF exposure region with a PB transmit power less than 51 dBm, equivalently power density smaller than 10 W/m^2 at 1 m from the PB [26]. We will discuss in detail later in the feasibility study in Section VI-E.

Insights: Fig. 4(a) shows that: (i) The channel coverage probability first slightly decreases and then increases with the increase of P_p. This can be explained as follows. At first, both the transmit power of the desired TX and the number of interfering TX increase with P_p. The interplay of this two factors results in the slightly decreasing trend for the channel coverage probability. As P_p further increases, the increase in the number of interfering TX is negligible, while the transmit power of the desired TX continues to increase, which leads to the increase of the channel coverage probability. (ii) The total coverage probability increases as PB transmit power P_p increases. When P_p is small, the desired TX might not receive enough power to activate the IT process. So the total coverage probability is small and is limited by the power coverage probability. When P_p is large, the channel coverage probability becomes the dominant factor in determining the total coverage probability. Hence, eventually the channel coverage probability and total coverage probability curves merge. (iii) The total coverage probability increase with $r_{\min}$, because more PBs falls into the LOS region and the path-loss is less severe, which improves the power coverage probability. The benefit of increasing the radius of the LOS region is less significant for the channel coverage probability.

C. Effect of Directional Beamforming at PB, TX and RX

Fig. 5 plots the total coverage probability and channel coverage probability against the power circuit activation threshold of TX for different beamforming parameters at TX and RX, i.e., [20 dB, −10 dB, 30°] and [10 dB, −10 dB, 45°].

1) Insights: Fig. 5 shows that, for both sets of beamforming parameters, as the power circuit activation threshold γ_{PT} increases, the channel coverage probability is always increasing, while the total coverage probability stays roughly the same at first and then decreases. This can be explained as follows. When γ_{PT} increases, the power coverage probability decreases. The reduction in the number of active TXs improves the channel coverage probability. With regards to the total coverage probability, its trend is determined by the interplay of channel coverage probability and power coverage probability. At first, the drop in power coverage is relatively small as shown in Fig. 2; so the total coverage probability is almost unchanged. After a certain point, the power coverage probability drops a lot, which mainly governs the total coverage probability. Hence, the total coverage probability decreases later on.

Comparing the curves for the different beamforming parameters, we can see that TX and RX with [20 dB, −10 dB, 30°] gives a higher total coverage probability in the low power circuit activation threshold region. This is because a narrower main lobe beam-width gives a larger main lobe gain and makes less interfering TXs fall into its main lobe which results in higher channel coverage probability. However, the total coverage probability is limited by the power coverage probability when γ_{PT} is large.

2) Impact of Number of Antenna Elements: The beamforming model adopted in this paper can be related to any specific

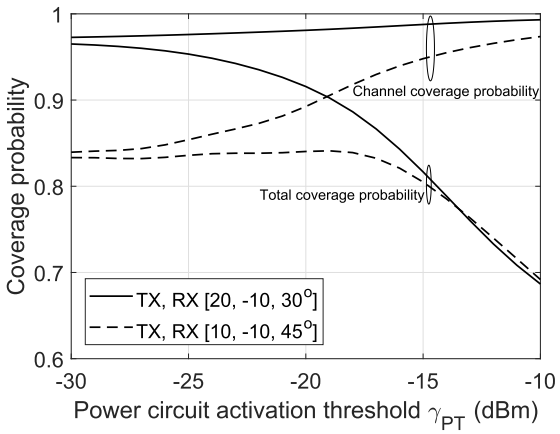

Fig. 5. Channel coverage probability and total coverage probability versus power circuit activation threshold γ_{PT} with different TX and RX beamforming parameters.

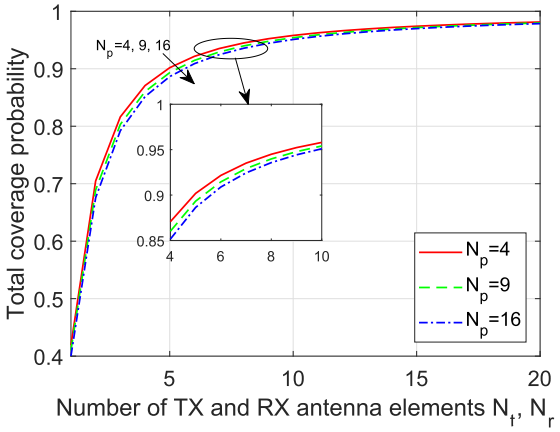

Fig. 6. Total coverage probability versus the numbers of antenna elements at TX and RX $\mathcal{N}_t$ and $\mathcal{N}_r$ with different numbers of antenna elements at PB.

array geometry by substituting the appropriate values for the three beamforming parameters. For instance, a uniform planar square array with half-wavelength antenna element spacing can be used at the PBs, TXs and RXs. The values for the main lobe antenna gain $G_a^{\max}$, side lobe antenna gain $G_a^{\min}$ and main lobe beamwidth θ_a depend on the number of the antenna elements $\mathcal{N}_a$ and can be calculated by using the equations below [18]:

$$G_a^{\max} = \mathcal{N}_a, \tag{27}$$

$$G_a^{\min} = \frac{\sqrt{\mathcal{N}_a} - \frac{\sqrt{3}}{2\pi}\mathcal{N}_a \sin(\frac{\sqrt{3}}{2\sqrt{\mathcal{N}_a}})}{\sqrt{\mathcal{N}_a} - \frac{\sqrt{3}}{2\pi}\sin(\frac{\sqrt{3}}{2\sqrt{\mathcal{N}_a}})}, \tag{28}$$

$$\theta_a = \frac{\sqrt{3}}{\sqrt{\mathcal{N}_a}}, \tag{29}$$

where $a = p$ for PB, $a = t$ for TX and $a = r$ for RX.

Fig. 6 plots the total coverage probability versus the numbers of antenna elements at the TX and RX $\mathcal{N}_t$ and $\mathcal{N}_r$ with different PB antenna element number $\mathcal{N}_p$. The figure shows that the total coverage probability increases with the numbers of antenna elements at the TX and RX, which agrees with our previous findings. However, under our considered system parameters, the total coverage probability stays roughly the same after having more than about 15 TX and RX antenna elements, as the side lobe antenna gain and the main lobe beamwidth stay almost constant with further increase in the number of antenna elements. In addition, the number of antenna elements at the PB does not significantly impact the total coverage probability.

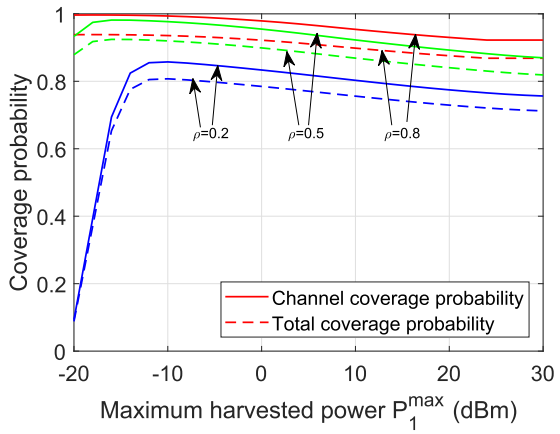

Fig. 7. Channel coverage probability and total coverage probability versus allowed maximum harvested power $P_1^{\max}$ with different time switching ratios.

D. Effect of Allowed Maximum Harvested Power at TX

Fig. 7 plots the total coverage probability and channel coverage probability against the allowed maximum harvested power of TX $P_1^{\max}$ for different time switching ratios 0.2, 0.5 and 0.8. Note that both the time switching ratio and the allowed maximum harvested power do not affect the power coverage probability.

Insights: Fig. 7 shows that the channel coverage probability and the total coverage probability both first increase with $P_1^{\max}$, then decrease. The rise of the channel coverage probability is because the possible transmit power of the desired TX increases with its allowed maximum harvested power. However, as $P_1^{\max}$ further increases, the accumulated harvested energy during the PT phase is higher and the transmit power of other active TX also goes up. As a result, the interfering power received at the RX is higher and the channel coverage probability decreases. The channel coverage probability will converge to a constant value as $P_1^{\max}$ increases even further, because the maximum transmit power of active TX has limited the channel performance.

Comparing the curves for different ρ, we can see that for a given maximum harvested power of TX $P_1^{\max}$, increasing ρ improves the coverage probabilities. When ρ is higher, more energy is captured during the PT phase. Therefore, the transmit power of active TX is now limited by the maximum transmit power $P_2^{\max}$. As a result, the channel coverage probability and total coverage probability converge and do not vary much with the changes in the allowed maximum harvested power.

E. Feasibility of PB-assisted mmWave Wireless Ad Hoc Networks

Finally, we investigate the feasibility of PB-assisted mmWave wireless ad hoc network. Fig. 8 is a plot of the total coverage probability and channel coverage probability

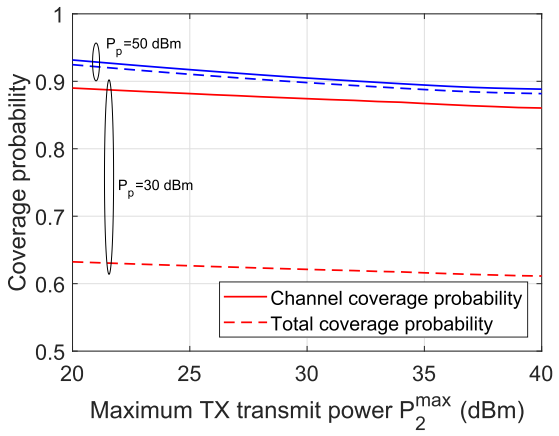

Fig. 8. Channel coverage probability and total coverage probability versus maximum TX transmit power $P_2^{\max}$ for different PB transmit power with the allowed maximum harvested power of TX being 50 dBm.

versus maximum TX transmit power $P_2^{\max}$ with varied PB transmit power, 50 dBm and 30 dBm. To better highlight the impact of the maximum transmit power at TX, we have set $P_1^{\max}$ equal to 50 dBm which is much higher than $P_2^{\max}$. From the figure, we can see that the channel coverage probability and total coverage probability do not change much with the considered maximum TX transmit power, which means that the probability mass function (PMF) of the transmit power for the desired TX remains almost the same. Note that the power coverage probability is independent of the maximum transmit power of TX.

Insight: From Fig. 8, the total coverage probability and the channel coverage probability are around 90% if P_p is 50 dBm. If PB transmits with a constant power of 50 dBm, the power density at a distant of 1 m from the PB is 7.95 W/m^2. This power density is smaller than 10 W/m^2, which is the permissible safety level of human exposure to RF electromagnetic fields based on IEEE Standard. Under this safety regulation, the maximum permissible PB transmit power would be 51 dBm. We have marked this value in Fig. 4(b). From Fig. 4(b), we can see that the total coverage probability with a PB transmit power less than 51 dBm can be up to 93.4% of the maximum system performance, as given by the asymptotic analysis in Section VI-B, based on our considered system parameters. The results in Fig. 4(b) and Fig. 8 show that PB-assisted mmWave ad hoc networks are feasible under practical network setup.

VII. Conclusion

In this paper, we have presented an approximate yet accurate model for PB-assisted mmWave wireless ad hoc networks, where TXs harvest energy from all PBs and then use the harvested energy to transmit information to their corresponding RXs. We first obtained the Laplace transform of the aggregate received power at the TX to compute the power coverage probability. Then, the channel coverage probability and total coverage probability were formulated based on discretizing the transmit power of TXs into a finite number of levels. The simulation results confirmed the accuracy of the proposed model. The results have shown that the total coverage probability improves by increasing the transmit power of PB, narrowing the main lobe beam-width and decreasing the maximum harvested power at the TX. Our results also showed that PB-assisted mmWave ad hoc network is feasible under realistic setup conditions. Future work can consider extensions to other MAC protocols such as carrier-sense multiple access (CSMA) [43], [44] and optimal allocation of the transmit power of an active TX.

$$
\begin{aligned}
\mathcal{L}_{P_{\mathrm{PT}}}(s) &= \mathbb{E}_{P_{\mathrm{PT}}}\left[\exp(-sP_{\mathrm{PT}})\right] \\
&= \mathbb{E}_{\phi_p,G_{i0},g_{i0}}\left[\exp\left(-sP_p\sum_{Z_i\in\phi_p}G_{i0}g_{i0}l(r_i)\right)\right] \\
&= \mathbb{E}_{\phi_p,G_{i0},g_{i0}}\left[\exp\left(-sP_p\sum_{0\leqslant r_i<1}G_{i0}g_{i0}l(r_i)\right)\right]\mathbb{E}_{\phi_p,G_{i0},g_{i0}}\left[\exp\left(-sP_p\sum_{1\leqslant r_i<r_{\min}}G_{i0}g_{i0}l(r_i)\right)\right] \\
&\quad\times\mathbb{E}_{\phi_p,G_{i0},g_{i0}}\left[\exp\left(-sP_p\sum_{r_{\min}\leqslant r_i<r_{\max}}G_{i0}g_{i0}l(r_i)\right)\right] \\
&= \underbrace{\exp\left(-\int_{-\pi}^{\pi}\int_{0}^{1}\mathbb{E}_{G_{i0},g_{i0}}[1-\exp(-sP_pG_{i0}g_{i0})]\lambda_p r\,dr\,d\theta\right)}_{A_1} \\
&\quad\times\underbrace{\exp\left(-\int_{-\pi}^{\pi}\int_{1}^{r_{\min}}\mathbb{E}_{G_{i0},g_{i0}}[1-\exp(-sP_pG_{i0}g_{i0}r^{-\alpha_{\mathrm{L}}})]\lambda_p r\,dr\,d\theta\right)}_{A_2} \\
&\quad\times\underbrace{\exp\left(-\int_{-\pi}^{\pi}\int_{r_{\min}}^{r_{\max}}\mathbb{E}_{G_{i0},g_{i0}}[1-\exp(-sP_pG_{i0}g_{i0}\beta r^{-\alpha_{\mathrm{N}}})]\lambda_p r\,dr\,d\theta\right)}_{A_3}.
\end{aligned}
\tag{30}
$$

APPENDIX A
PROOF OF THEOREM 1

Following the definition of Laplace transform, the Laplace transform of the aggregate received power can be expressed as (30), as shown at the bottom of the previous page.

The first term A_1 is evaluated as follows

$$\begin{aligned} A_1 &= \exp\left(-\pi\lambda_p\left(1-\mathbb{E}_{G_{i0},g_{i0}}[\exp(-sP_pG_{i0}g_{i0})]\right)\right) \\ &= \exp\left(-\pi\lambda_p\left(1-\mathbb{E}_{G_{i0}}\left[\int_0^\infty \exp(-sP_pG_{i0}g) f_{g_{\mathrm{L}}}(g)dg\right]\right)\right) \\ &= \exp\left(-\pi\lambda_p + \pi\lambda_p m^m \mathbb{E}_{G_{i0}}\left[(m+sP_pG_{i0})^{-m}\right]\right) \\ &= \exp\left(-\pi\lambda_p + \pi\lambda_p m^m \sum_{k=1}^{4}(m+sP_pG_k)^{-m}p_k\right), \end{aligned} \quad (31)$$

where we use the fact that the link in LOS state experiences Nakagami-m fading with $f_{g_{\mathrm{L}}}(g) = \frac{m^m g^{m-1}\exp(-mg)}{\Gamma(m)}$.

The second term A_2 is evaluated as follows

$$\begin{aligned} A_2 = \exp\Big(&\pi\lambda_p\mathbb{E}_{G_{i0},g_{i0}}\left[1-\exp(-sP_pG_{i0}g_{i0})\right] \\ &-\pi\lambda_p r_{\min}^2\mathbb{E}_{G_{i0},g_{i0}}\left[1-\exp(-sr_{\min}^{-\alpha_{\mathrm{L}}}P_pG_{i0}g_{i0})\right] \\ &-\pi\lambda_p\mathbb{E}_{G_{i0},g_{i0}}\left[(sP_pG_{i0})^{\delta_{\mathrm{L}}}g_{i0}^{\delta_{\mathrm{L}}}\gamma(1-\delta_{\mathrm{L}},sP_pg_{i0}G_{i0})\right] \\ &+\pi\lambda_p \\ &\times\mathbb{E}_{G_{i0},g_{i0}}\left[(sP_pG_{i0})^{\delta_{\mathrm{L}}}g_{i0}^{\delta_{\mathrm{L}}}\gamma(1-\delta_{\mathrm{L}},sP_pg_{i0}G_{i0}r_{\min}^{-\alpha_{\mathrm{L}}})\right]\Big) \end{aligned} \quad (32a)$$

$$\begin{aligned} = \exp\Big(&\pi\lambda_p - \pi\lambda_p m^m\sum_{k=1}^{4}(m+sP_pG_k)^{-m}p_k \\ &-\pi\lambda_p r_{\min}^2 + \sum_{k=1}^{4}\pi\lambda_p r_{\min}^2 m^m(m+sr_{\min}^{-\alpha_{\mathrm{L}}}P_pG_k)^{-m}p_k \\ &+\pi\lambda_p\sum_{k=1}^{4}\left(sP_pG_k\right)^{\delta_{\mathrm{L}}}\frac{m^m(sP_pG_k)^{-\delta_{\mathrm{L}}-m}\alpha_{\mathrm{L}}\Gamma(1+m)}{(2+m\alpha_{\mathrm{L}})\Gamma(m)} \\ &\times{}_2F_1\left(1+m,m+\delta_{\mathrm{L}};1+m+\delta_{\mathrm{L}};-\frac{m}{sP_pG_k}\right)p_k \\ &-\pi\lambda_p\sum_{k=1}^{4}\left(sP_pG_k\right)^{\delta_{\mathrm{L}}} \\ &\times\frac{m^m(r_{\min}^{-\alpha_{\mathrm{L}}}sP_pG_k)^{-\delta_{\mathrm{L}}-m}\alpha_{\mathrm{L}}\Gamma(1+m)}{(2+m\alpha_{\mathrm{L}})\Gamma(m)} \\ &\times{}_2F_1\left(1+m,m+\delta_{\mathrm{L}};1+m+\delta_{\mathrm{L}};-\frac{r_{\min}^{\alpha_{\mathrm{L}}}m}{sP_pG_k}\right)p_k\Big), \end{aligned} \quad (32b)$$

where (32a) follows from changing variables and integration by parts and (32b) is obtained after taking the expectation over g_{L} then G_{i0}.

Similarly, the third term A_3 can be worked out by taking the expectation over g_{N}, which has a PDF as $f_{g_{\mathrm{N}}}(g) = \exp(-g)$. The details are omitted for sake of brevity. Finally, the Laplace transform in Theorem 1 is obtained by substituting A_1, A_2 and A_3 into (30).

APPENDIX B
PROOF OF PROPOSITION 1

By substituting (15) into (16), we can express the conditional channel coverage probability as

$$\begin{aligned} &\mathbb{P}_{\mathrm{cov}}^{C}(\gamma_{\mathrm{TR}}) \\ &= \Pr\left(\frac{P_{X_0}D_0\ h_0\ l(d_0)}{\sum_{X_i\in\phi_{\mathrm{active}}}P_{X_i}D_{i0}h_{i0}l(X_i)+\sigma^2} > \gamma_{\mathrm{TR}}\right) \\ &\approx \Pr\left(\frac{P_{X_0}D_0\ h_0\ l(d_0)}{\sum_{n=0}^{N}\sum_{X_i\in\phi_t^n}P_t^nD_{i0}h_{i0}l(X_i)+\sigma^2} > \gamma_{\mathrm{TR}}\right) \quad (33a) \\ &= \Pr\left(h_0 > \frac{\gamma_{\mathrm{TR}}(I_X+\sigma^2)}{P_{X_0}D_0\ l(d_0)}\right) \\ &= \mathbb{E}_{P_{X_0},I_X}\left[1-F_{h_0}\left(\frac{\gamma_{\mathrm{TR}}(I_X+\sigma^2)}{P_{X_0}D_0l(d_0)}\right)\right], \quad (33b) \end{aligned}$$

where approximation in (33a) comes from our power level discretization, $I_X = \sum_{n=0}^{N}\sum_{X_i\in\phi_t^n}P_t^nD_{i0}h_{i0}l(X_i)$ and $F_{h_0}(\cdot)$ is the CDF of the fading power gain on the reference TX-RX link. Since the desired link is assumed to experience Nakagami-m fading with integer m, the CDF of h_0 has a nice form, which is $F_{h_0}(h) = 1-\sum_{l=0}^{m-1}\frac{1}{l!}(mh)^l\exp(-mh)$. Hence, we can re-write (33b) as

$$\begin{aligned} &\mathbb{P}_{\mathrm{cov}}^{C}(\gamma_{\mathrm{TR}}) \\ &= \mathbb{E}_{P_{X0},I_X}\left[\sum_{l=0}^{m-1}\frac{1}{l!}\left(m\frac{\gamma_{\mathrm{TR}}(I_X+\sigma^2)}{P_{X_0}D_0\ l(d_0)}\right)^l\right. \\ &\qquad\left.\times\exp\left(-m\frac{\gamma_{\mathrm{TR}}(I_X+\sigma^2)}{P_{X_0}D_0\ l(d_0)}\right)\right] \\ &= \sum_{n=0}^{N}\sum_{l=0}^{m-1}\frac{1}{l!}\mathbb{E}_{I_X}\left[\left(m\frac{\gamma_{\mathrm{TR}}(I_X+\sigma^2)}{P_t^nD_0l(d_0)}\right)^l\right. \\ &\qquad\left.\times\exp\left(-m\frac{\gamma_{\mathrm{TR}}(I_X+\sigma^2)}{P_t^nD_0l(d_0)}\right)\right]\frac{k_n}{\mathbb{P}_{\mathrm{cov}}^{P}(\gamma_{\mathrm{PT}})}, \end{aligned} \quad (34)$$

where the PMF of P_{X_0} is $\Pr(P_{X_0} = P_t^n) = \frac{k_n}{\mathbb{P}_{\mathrm{cov}}^{P}(\gamma_{\mathrm{PT}})}$ in (34), as we assume that the desired TX is active.

The general form of the Laplace transform of $I_X+\sigma^2$ is $\mathcal{L}_{I_X+\sigma^2}(s) = \mathbb{E}_{I_X}[\exp(-s(I_X+\sigma^2))]$. Taking lth derivative with respect to s, we achieve

$$\begin{aligned} \frac{dl}{ds^l}\mathcal{L}_{I_X+\sigma^2}(s) &= \mathbb{E}_{I_X}\left[\frac{dl}{ds^l}\exp(-s(I_X+\sigma^2))\right] \\ &= \mathbb{E}_{I_X}\left[(-I_X-\sigma^2)^l\exp(-s(I_X+\sigma^2))\right]. \end{aligned} \quad (35)$$

Comparing (35) with the expectation term in (34), we have

$$\mathbb{P}_{\mathrm{cov}}^{C}(\gamma_{\mathrm{TR}}) = \sum_{n=0}^{N}\sum_{l=0}^{m-1}\frac{(-s)^l}{l!}\frac{dl}{ds^l}\mathcal{L}_{I_X+\sigma^2}(s)\frac{k_n}{\mathbb{P}_{\mathrm{cov}}^{P}(\gamma_{\mathrm{PT}})}, \quad (36)$$

where $s = \frac{m\gamma_{\mathrm{TR}}}{P_t^nD_0l(d_0)}$. Hence, we arrive the result in Proposition 1.

REFERENCES

[1] X. Lu, P. Wang, D. Niyato, D. I. Kim, and Z. Han, "Wireless networks with RF energy harvesting: A contemporary survey," *IEEE Commun. Surveys Tuts.*, vol. 17, no. 2, pp. 757–789, 2nd Quart., 2015.

[2] H. Tabassum, E. Hossain, A. Ogundipe, and D. I. Kim, "Wireless-powered cellular networks: Key challenges and solution techniques," *IEEE Commun. Mag.*, vol. 53, no. 6, pp. 63–71, Jun. 2015.

[3] Y. Zeng, B. Clerckx, and R. Zhang, "Communications and signals design for wireless power transmission," *IEEE Trans. Commun.*, vol. 65, no. 5, pp. 2264–2290, May 2017.

[4] R. Zhang and C. K. Ho, "MIMO broadcasting for simultaneous wireless information and power transfer," *IEEE Trans. Wireless Commun.*, vol. 12, no. 5, pp. 1989–2001, May 2013.

[5] A. A. Nasir, X. Zhou, S. Durrani, and R. A. Kennedy, "Relaying protocols for wireless energy harvesting and information processing," *IEEE Trans. Wireless Commun.*, vol. 12, no. 7, pp. 3622–3636, Jul. 2013.

[6] (Mar. 2017). *CES 2017 Innovation Awards*. [Online]. Available: http://www.ces.tech/Events-Experiences/Innovation-Awards-Program/Honorees.aspx

[7] Y. Ma, H. Chen, Z. Lin, Y. Li, and B. Vucetic, "Distributed and optimal resource allocation for power beacon-assisted wireless-powered communications," *IEEE Trans. Commun.*, vol. 63, no. 10, pp. 3569–3583, Oct. 2015.

[8] C. Zhong, X. Chen, Z. Zhang, and G. K. Karagiannidis, "Wireless-powered communications: Performance analysis and optimization," *IEEE Trans. Commun.*, vol. 63, no. 12, pp. 5178–5190, Dec. 2015.

[9] X. Jiang, C. Zhong, Z. Zhang, and G. K. Karagiannidis, "Power beacon assisted wiretap channels with jamming," *IEEE Trans. Wireless Commun.*, vol. 15, no. 12, pp. 8353–8367, Dec. 2016.

[10] K. Huang and V. K. N. Lau, "Enabling wireless power transfer in cellular networks: Architecture, modeling and deployment," *IEEE Trans. Wireless Commun.*, vol. 13, no. 2, pp. 902–912, Feb. 2014.

[11] S. Lee, R. Zhang, and K. Huang, "Opportunistic wireless energy harvesting in cognitive radio networks," *IEEE Trans. Wireless Commun.*, vol. 12, no. 9, pp. 4788–4799, Sep. 2013.

[12] Z. Wang, L. Duan, and R. Zhang, "Adaptively directional wireless power transfer for large-scale sensor networks," *IEEE J. Sel. Areas Commun.*, vol. 34, no. 5, pp. 1785–1800, May 2016.

[13] Y. Liu, L. Wang, S. A. R. Zaidi, M. Elkashlan, and T. Q. Duong, "Secure D2D communication in large-scale cognitive cellular networks: A wireless power transfer model," *IEEE Trans. Commun.*, vol. 64, no. 1, pp. 329–342, Jan. 2016.

[14] J. Guo, S. Durrani, X. Zhou, and H. Yanikomeroglu, "Outage probability of ad hoc networks with wireless information and power transfer," *IEEE Wireless Commun. Lett.*, vol. 4, no. 4, pp. 409–412, Aug. 2015.

[15] T. S. Rappaport *et al.*, "Millimeter wave mobile communications for 5G cellular: It will work!" *IEEE Access*, vol. 1, pp. 335–349, May 2013.

[16] J. G. Andrews, T. Bai, M. N. Kulkarni, A. Alkhateeb, A. K. Gupta, and R. W. Heath, Jr., "Modeling and analyzing millimeter wave cellular systems," *IEEE Trans. Commun.*, vol. 65, no. 1, pp. 403–430, Jan. 2017.

[17] M. Di Renzo, "Stochastic geometry modeling and analysis of multi-tier millimeter wave cellular networks," *IEEE Trans. Wireless Commun.*, vol. 14, no. 9, pp. 5038–5057, Sep. 2015.

[18] K. Venugopal, M. C. Valenti, and R. W. Heath, Jr., "Device-to-device millimeter wave communications: Interference, coverage, rate, and finite topologies," *IEEE Trans. Wireless Commun.*, vol. 15, no. 9, pp. 6175–6188, Sep. 2016.

[19] D. Maamari, N. Devroye, and D. Tuninetti, "Coverage in mmWave cellular networks with base station co-operation," *IEEE Trans. Wireless Commun.*, vol. 15, no. 4, pp. 2981–2994, Apr. 2016.

[20] T. A. Khan, A. Alkhateeb, and R. W. Heath, Jr., "Millimeter wave energy harvesting," *IEEE Trans. Wireless Commun.*, vol. 15, no. 9, pp. 6048–6062, Sep. 2016.

[21] L. Wang, M. Elkashlan, R. W. Heath, Jr., M. Di Renzo, and K.-K. Wong, "Millimeter wave power transfer and information transmission," in *Proc. IEEE GLOBECOM*, Dec. 2015, pp. 1–6.

[22] X. Zhou, S. Durrani, and J. Guo, "Characterization of aggregate received power from power beacons in millimeter wave ad hoc networks," in *Proc. IEEE ICC*, May 2017, pp. 1–7.

[23] A. Biason and M. Zorzi, "Joint transmission and energy transfer policies for energy harvesting devices with finite batteries," *IEEE J. Sel. Areas Commun.*, vol. 33, no. 12, pp. 2626–2640, Dec. 2015.

[24] A. Ghazanfari, H. Tabassum, and E. Hossain, "Ambient RF energy harvesting in ultra-dense small cell networks: Performance and trade-offs," *IEEE Wireless Commun.*, vol. 23, no. 2, pp. 38–45, Apr. 2016.

[25] E. Boshkovska, D. W. K. Ng, N. Zlatanov, and R. Schober, "Practical non-linear energy harvesting model and resource allocation for SWIPT systems," *IEEE Commun. Lett.*, vol. 19, no. 12, pp. 2082–2085, Dec. 2015.

[26] M. Xia and S. Aissa, "On the efficiency of far-field wireless power transfer," *IEEE Trans. Signal Process.*, vol. 63, no. 11, pp. 2835–2847, Jun. 2015.

[27] M. Di Renzo, W. Lu, and P. Guan, "The intensity matching approach: A tractable stochastic geometry approximation to system-level analysis of cellular networks," *IEEE Trans. Wireless Commun.*, vol. 15, no. 9, pp. 5963–5983, Sep. 2016.

[28] T. Bai and R. W. Heath, Jr., "Coverage and rate analysis for millimeter-wave cellular networks," *IEEE Trans. Wireless Commun.*, vol. 14, no. 2, pp. 1100–1114, Feb. 2015.

[29] M. Di Renzo and W. Lu, "System-level analysis and optimization of cellular networks with simultaneous wireless information and power transfer: Stochastic geometry modeling," *IEEE Trans. Veh. Technol.*, vol. 66, no. 3, pp. 2251–2275, Mar. 2017.

[30] M. R. Akdeniz *et al.*, "Millimeter wave channel modeling and cellular capacity evaluation," *IEEE J. Sel. Areas Commun.*, vol. 32, no. 6, pp. 1164–1179, Jun. 2014.

[31] X. Zhang and J. G. Andrews, "Downlink cellular network analysis with multi-slope path loss models," *IEEE Trans. Commun.*, vol. 63, no. 5, pp. 1881–1894, May 2015.

[32] S. Al-Ahmadi and H. Yanikomeroglu, "On the approximation of the generalized-K distribution by a gamma distribution for modeling composite fading channels," *IEEE Trans. Wireless Commun.*, vol. 9, no. 2, pp. 706–713, Feb. 2010.

[33] G. Lee, Y. Sung, and J. Seo, "Randomly-directional beamforming in millimeter-wave multiuser MISO downlink," *IEEE Trans. Wireless Commun.*, vol. 15, no. 2, pp. 1086–1100, Feb. 2016.

[34] M. Haenggi, *Stochastic Geometry for Wireless Networks*. Cambridge, U.K.: Cambridge Univ. Press, 2013.

[35] A. Thornburg, T. Bai, and R. W. Heath, Jr., "Performance analysis of outdoor mmWave ad hoc networks," *IEEE Trans. Signal Process.*, vol. 64, no. 15, pp. 4065–4079, Aug. 2016.

[36] M. Di Renzo and P. Guan, "Stochastic geometry modeling of coverage and rate of cellular networks using the Gil-Pelaez inversion theorem," *IEEE Commun. Lett.*, vol. 18, no. 9, pp. 1575–1578, Sep. 2014.

[37] Y.-C. Ko, M. S. Alouini, and M. K. Simon, "Outage probability of diversity systems over generalized fading channels," *IEEE Trans. Commun.*, vol. 48, no. 11, pp. 1783–1787, Nov. 2000.

[38] J. Guo, S. Durrani, and X. Zhou, "Outage probability in arbitrarily-shaped finite wireless networks," *IEEE Trans. Commun.*, vol. 62, no. 2, pp. 699–712, Feb. 2014.

[39] I. S. Gradshteyn and I. M. Ryzhik, *Table of Integrals, Series, and Products*, 7th ed. San Diego, CA, USA: Academic, 2007.

[40] S. Akbar, Y. Deng, A. Nallanathan, M. Elkashlan, and A.-H. Aghvami, "Simultaneous wireless information and power transfer in K-tier heterogeneous cellular networks," *IEEE Trans. Wireless Commun.*, vol. 15, no. 8, pp. 5804–5818, Aug. 2016.

[41] A. H. Sakr and E. Hossain, "Analysis of K-tier uplink cellular networks with ambient RF energy harvesting," *IEEE J. Sel. Areas Commun.*, vol. 33, no. 10, pp. 2226–2238, Oct. 2015.

[42] A. H. Sakr and E. Hossain, "Cognitive and energy harvesting-based D2D communication in cellular networks: Stochastic geometry modeling and analysis," *IEEE Trans. Commun.*, vol. 63, no. 5, pp. 1867–1880, May 2015.

[43] H. ElSawy and E. Hossain, "A modified hard core point process for analysis of random CSMA wireless networks in general fading environments," *IEEE Trans. Commun.*, vol. 61, no. 4, pp. 1520–1534, Apr. 2013.

[44] M. Kaynia, N. Jindal, and G. E. Øien, "Improving the performance of wireless ad hoc networks through MAC layer design," *IEEE Trans. Wireless Commun.*, vol. 10, no. 1, pp. 240–252, Jan. 2011.

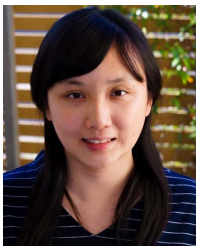

Xiaohui Zhou (S'15) received the B.Eng. degree (Hons.) from The Australian National University, Canberra, Australia, in 2014, where she is currently pursuing the Ph.D. degree with the Research School of Engineering. She was a recipient of the ANU University Research Scholarship. Her research interests include wireless power transfer, stochastic geometry, and fifth-generation wireless networks.

Jing Guo (S'12–M'17) received the B.Sc. degree (Hons.) in electronics and telecommunications engineering from The Australian National University, Australia, and the Beijing Institute of Technology, China, in 2012, and the Ph.D. degree in telecommunications engineering from The Australian National University in 2016. She is currently a Research Fellow with the Research School of Engineering, The Australian National University. Her research interest lies in the field of wireless communications, including machine-to-machine communications and the application of stochastic geometry to wireless networks.

Salman Durrani (S'00–M'05–SM'10) received the B.Sc. degree (Hons.) in electrical engineering from the University of Engineering & Technology, Lahore, Pakistan, in 2000, and the Ph.D. degree in electrical engineering from The University of Queensland, Brisbane, Australia, in 2004. He has been with The Australian National University, Canberra, Australia, since 2005, where he is currently an Associate Professor with the Research School of Engineering, College of Engineering and Computer Science. His research interests are in wireless communications and signal processing, including machine-to-machine and device-to-device communications, wireless energy harvesting systems, stochastic geometry modeling of finite area networks, and synchronization in communication systems.

Marco Di Renzo (S'05–AM'07–M'09–SM'14) received the Laurea degree (*cum laude*) and the Ph.D. degree in electrical engineering from the University of L'Aquila, Italy, in 2003 and 2007, respectively, and the D.Sc. degree (HDR) from the University of Paris-Sud, Paris, France, in 2013. Since 2010, he has been a CNRS Associate Professor (Chargé de Recherche Titulaire CNRS) with the Laboratory of Signals and Systems, Paris-Saclay University–CNRS, CentraleSupélec, University of Paris-Sud. He is currently an Adjunct Professor with the University of Technology Sydney, Australia, a Visiting Professor with the University of L'Aquila, Italy, and a Co-Founder of the university spin-off company WEST Aquila s.r.l., Italy. He was a recipient of several awards, including the 2013 IEEE-COMSOC Best Young Researcher Award for Europe, Middle East, and Africa (EMEA Region), the 2014–2015 Royal Academy of Engineering Distinguished Visiting Fellowship, and the 2015 IEEE Jack Neubauer Memorial Best System Paper Award. He is a recipient of the 2015–2018 CNRS Award for Excellence in Research and in Advising Doctoral Students. He serves as an Associate Editor-in-Chief of the IEEE COMMUNICATIONS LETTERS, and an Editor of the IEEE TRANSACTIONS ON COMMUNICATIONS, and the IEEE TRANSACTIONS ON WIRELESS COMMUNICATIONS. He is also a Distinguished Lecturer of the IEEE Vehicular Technology Society and the IEEE Communications Society.